Magnetite (Fe3O4) nanoparticles as adsorbents for As and Cu removal

Simona Liliana Iconaru, Régis Guégan, Cristina Liana Popa, Mikael Motelica-Heino, Carmen Steluta Ciobanu, Daniela Predoi

Magnetite (Fe_3O_4) nanoparticles as adsorbents for As and Cu removal

Simona Liliana Iconaru[a], Régis Guégan[b], Cristina Liana Popa[a], Mikael Motelica-Heino[b]*, Carmen Steluta Ciobanu[a], Daniela Predoi[a*]

[a]National Institute of Materials Physics, 077125, Magurele Romania

[b]ISTO UMR 7327 CNRS Université d'Orléans, France

Correspondence should be addressed to Mikael Motelica-Heino; mikael.motelica@univ-orleans.fr and Daniela Predoi; dpredoi@gmail.com

Abstract

The aim of this study was to develop synthetic magnetite nanoparticles (nFe_3O_4) with preferential reactivity for trace elements (TE) for possible environmental applications as adsorbents. The synthetic magnetite materials obtained through the co-precipitation of both Fe^{3+} and Fe^{2+} ions (Fe^{2+} / Fe^{3+} = 0.5) were characterized by a set of complementary techniques such as X-ray diffraction, transmission and scanning electron microscopy, Fourier transform infrared and Raman spectroscopy, and BET adsorption method. The resulting nFe_3O_4 displayed a wide specific surface area (100 m^2 g^{-1}) with particles reaching a size of about 10 nm, smaller than those of the well-crystallized commercial ones (cFe_3O_4) estimated at 80 nm while showing a BET surface area of 6.8 m^2 g^{-1}. The adsorption properties of the synthetic nFe_30_4 magnetite nanoparticles were characterized and compared to commercial analogues with the adsorption of both arsenic and copper. The equilibrium adsorption isotherms were properly fitted with Langmuir and Freundlich equation models. The maximum adsorption capacity for the solid phase, q_m, obtained for the adsorption of arsenic onto nFe_3O_4 had an increase of 69.46% comparative to the value obtained for the adsorption of arsenic on cFe_3O_4. The results suggested that the iron oxide nanoparticles

displayed a definitive potential for removal and/or immobilization of TE from contaminated waters and/or soils.

Keywords*: Arsenic, Copper, Magnetite, Nanoparticles, Adsorption*

1. Introduction

Water is vital for all known forms of life and a valuable resource to human civilization. Providing clean and affordable water to meet human needs is a major challenge of the 21st century. Unfortunately, rapid technological and industrial development in recent decades has led to a number of environmental problems, particularly with regard to the pollution of water resources. In this context, trace elements (TE) are one of the major classes of pollutants responsible for imbalances in aquatic ecosystems. Generally, TE present in wastewaters, soils and even tap waters originate from industrial and municipal wastes as well as excessive utilization of pesticides and herbicides (Zhu et al., 2015). Frequent exposures to high concentration of TE have been recognized to lead to various health problems such as diarrhea, hemolysis, perturbation of the central nervous system (Cho et al., 2012; Barbuceanu et al., 2015; Dalida et al., 2011). Also, Cu and As poisoning can lead to cancer, skin diseases, hyperkeratosis, etc. (Cho et al., 2012; Tuna et al., 2013; Yang et al., 2015). Thus, health authorities such as the United States Environmental Protection Agency (USEPA) set the maximum levels for copper and arsenic in drinking waters to be 1.3 and 0.01 mg L^{-1} (He and Charlet, 2013). One of the most toxic elements, also classified as the world's most hazardous chemical is arsenic (USEPA, 2003). The occurrence of arsenic in the water supply of numerous countries represents a worldwide health risk to both humans and animals. Arsenic is present in water in inorganic form as arsenate (As(V)) and arsenite (As(III)). While arsenate is the most predominant form of arsenic and it is present in well-oxygenated waters (Ferguson et al.,

1972), As(III) is the dominant form of arsenic in groundwaters (Smedley and Kinniburgh, 2002). In water, As(III) is much more toxic, more soluble, and more mobile than As(V) (Kanel et al., 2006; Zhang et al., 2007), therefore representing a dangerous threat to human health.

One of the most effective principles for removing inorganic pollutants such as TE as well as organic ones is adsorption. In order to have the desired effects, the adsorbent materials must possess specific properties like a large specific area and an excellent affinity to micro-pollutants. Natural materials such as activated carbon, clay minerals, zeolites and iron oxides are already being used for water remediation (Boneto et al., 2015; Guégan et al, 2015; Thiebault et al., 2015). Although activated carbon presents excellent adsorption properties, the costs involved in using this type of material can be very high. Some of the major drawbacks of activated carbon are the high costs of carbon replacement, the production of dimethyl disulfide as a byproduct of catalytic carbons, the carbon disposal or the decrease of its TE adsorption capacity due to the adsorption of air moisture (http://www.odor.net/carbon-adsorption/).

Recently, adsorbents with magnetic properties have attracted much attention from researchers due to a significant effect in accelerating separation and improving the efficiency of water treatment (Sivashankar et al., 2014; Harikishore et al., 2016; Mehta et al., 2015; Gomez-Pastora et al., 2014). The iron oxide nanoparticles attracted considerable attention for a variety of fundamental and technological applications such as novel optical electrical and magnetic properties due to the surface /volume ratio at the nanomatric scale. According to the studies conducted by Hochella et al. (2005), at many kilometers downstream from mining sites, iron oxide particles at nanomatric scale with various surface-bound metals were found. The new findings suggested the importance of magnetic iron nanoparticles in a variety of geochemical processes such as the sorption of trace elements, photochemical reduction, acceptance of electrons from

microbial respiration and heterogeneous catalysis. Therefore, these nanoparticles received significant attention for potential applications in the marine environment, site remediation and groundwater treatment (Gilbert and Banfield, 2005; Brown Jr. and Parks, 2001). In general, the results have shown that it is possible to produce promising adsorbents in this field creating new options for the adsorption of both TE and organic pollutants. In this context, in the last decade the adsorption capacity of As and Cu by iron oxide based materials (hematite, goethite, limonite, siderite and magnetite) has been widely investigated (Lunge et al., 2014; Mayo et al., 2007; Savage and Diallo, 2005; Wang et al., 2011; Wiatrowski et al., 2009). Moreover, the most promising results on the adsorption capacity of As and Cu from aqueous solutions have been obtained for magnetic iron oxide nanoparticles.

For this purpose, synthetic magnetic nanoparticles (nFe_3O_4) have been developed based on a co-precipitation method at room temperature in controlled Ar atmosphere and their adsorption properties for As and Cu were studied and compared to those of a commercial analogous material (cFe_3O_4).

2. Materials and Methods

2.1. Materials

Ferrous chloride tetrahydrate ($FeCl_24H_2O$), ferric chloride hexahydrate ($FeCl_36H_2O$), sodium hydroxide (NaOH) and hydrochloric acid (HCl) were purchased from Merck (Darmstadt, Germany). Commercial magnetite (cFe_3O_4) was purchased from Sigma Aldrich (637106). Arsenic standard solution (1000 mg L^{-1} (As^{3+})) and Coper standard solution used in the batch experiments (1000 mg L^{-1} Cu^{2+})) were purchased from CHEM-LAB. Deionized water was used in the synthesis of the samples and for the preparation of arsenic and copper containing solutions.

2.2. Magnetite adsorbents

Commercial magnetite (cFe_3O_4) used in the experiments was purchased from Sigma Aldrich (637106- 97% Fe_3O_4). The structural information (XRD) for cFe_3O_4 powders provided by Sigma Aldrich classified the sample as magnetite with a cubic structure of the Fd3m (227) space group, in good agreement with the JCPDS card number 19-629.

Synthesized magnetite (nFe_3O_4) was prepared in a controlled atmosphere (Ar) by a co-precipitation method. In order to obtain magnetite at a nanometric scale, ferrous chloride tetrahydrate ($FeCl_2 \cdot 4H_2O$) dissolved in 50 mL 2 M HCl was mixed with 60 mL ferric chloride hexahydrate ($FeCl_3 \cdot 6H_2O$) at room temperature (Fe^{2+}/Fe^{3+}=0.5) (Massart, 1982; Massart, 1979; Predoi, 2007). The solution mixture was added drop by drop into a 200 mL NaOH 5M solution under vigorous stirring for about 1 h.

With the use a magnet, the formed black precipitate was isolated by decantation, then separated by a centrifugation process (10000 rpm) and washed with deionised water. The final material was dried at 40 ^oC for 24 h in an oven.

2.3. Characterization methods

The X-Ray Diffraction patterns of cFe_3O_4 and nFe_3O_4 samples were recorded with a Bruker D8 Advance diffractometer, with a high efficiency one-dimensional detector (Lynx Eye type) operated in integration mode, using a nickel filtered Cu K_α (λ=1.5418 Å) radiation. The diffraction patterns were collected with a step of 0.02° and a 34 s measuring time per step in the 2θ range 20°-70°. The morphology of the samples was obtained by scanning electron microscopy, using a Quanta Inspect F50 microscope with a field emission gun (FEG). The microscope was also equipped with an energy dispersive X-ray (EDAX) attachment used to identify the elemental composition of the materials. Transmission electron microscopy (TEM) investigations were performed with a CM 20 (Philips- FEI) Transmission Electron Microscope equipped with a Lab6

filament operating at 200 kV. The powders were dispersed in ethanol in an ultrasonic bath for approximately 5 minutes. Afterwards, 5µl of suspension was deposited on a microscopy copper grill previously coated with carbon. The copper grills were then observed at the microscope. The particle size was measured by the SZ-100 Nanoparticle Analyzer (Horiba) using dynamic light scattering (DLS). The signal obtained from the scattered light is fed into a multichannel correlator that generates a function used to determine the translational diffusion coefficient of the analysed particles. The Stokes-Einstein equation is then used to calculate the particle size. Attenuated total reflectance Fourier transform infrared spectroscopy (ATR-FTIR) was used in order to establish the functional groups present in the prepared powders. The spectra were recorded with a SP 100 Perkin Elmer spectrophotometer in transmission mode. Each spectrum was acquired in the 2000-400 cm^{-1} spectral range using a Diamond/KRS-5 crystal cell with a resolution of 4 cm^{-1}. For the Raman spectra acquisition, a Renishaw InVia dispersive Raman spectrometer equipped with a Leica DM microscope and a 514 nm (gas-type) Spectra Physics Ar ion laser (20 mW) was used. The samples were analyzed using 1800 l/mm gratings and a 514 nm laser at a power of 0.2 mW. The spectra were acquired in the spectral range 100-2000 cm^{-1} with a resolution below 2 cm^{-1}. Micromeritics ASAP 2020 Physisorption Analyzer (Micromeritics Instrument Corp.) was used to determine surface area, pore size and pore volume of cFe_3O_4 and nFe_3O_4 by nitrogen adsorption at 77 K. The cFe_3O_4 and nFe_3O_4 powders (about 0.20 g each) were degassed overnight being heated at 100 ^oC prior to measurements of the surface area, pore volume, and average pore diameter. The specific BET surface area of both cFe_3O_4 and nFe_3O_4 samples were determined by the classic Brunauer Emmett Teller (BET) method (Brunauer et al., 1938). The concentration of As^{3+} and Cu^{2+} from the aqueous solutions was determined by Flame Atomic Absorption Spectrometry (AAS) using a Zeeman HITACHI Z-8100. An atomizer with an air/acetylene burner

was used for determining the arsenic and copper concentrations. The operating settings were those recommended in the manual. The wavelengths used were 193.7 and 193.7 nm for As and Cu, respectively.

2.4. Equilibrium adsorption experiments

Batch equilibrium adsorption isotherms were conducted with aqueous solutions containing As and Cu at a concentration range 0.1-150 mg L^{-1}. The batch adsorption experiments were carried out in 40 ml silicon tubes. The amount of adsorbent used was 0.2 g and the solution pH was adjusted to 5 by the addition of 0.1 M hydrochloric acid (HCl). A pH around 5 was chosen in these experiments in agreement with previous studies (Panday et al., 1985) that showed that the degree of removal of pollutants increases when the pH of the solution increases from 3.0 to 8.0. According to Elliott and Huang (Elliott and Huang, 1981), the removal of a substance that pollutes continental and/or oceanic waters is greatly dependent on pH of the solution which alters the surface charge of the adsorbent and the ionisation degree of the adsorbate. The solution volume was kept at 20 ml and the mixture was stirred on a Mixer SRT1 Roller for 24 h. After stirring for 24 h, the tubes were centrifuged for 30 min at 10000 rpm. The supernatant was filtered and analyzed by Atomic Absorption Spectrometry (AAS) and the recovered powders were also characterized. The batch experiments were carried out in triplicate and at room temperature. All absorbance readings were also done in triplicates. The AAS measurements were performed using a 193.7 nm wavelength for arsenic and 324.7 nm wavelength for cooper. The structure and morphology of the rerecovered powders were caracterized by XRD, SEM and EDX method while the optical properties were investigated using FTIR and Raman spectroscopy.

3. Results and discussions

3.1. Characteristics of the synthesized magnetite nano-particles

The X-ray diffraction pattern (Figure 1A-B) of commercial magnetite (cFe_3O_4) and synthesized magnetite displayed different peaks at about 30, 35, 43, 54, 57 and 63° (2θ), characteristics to a spinel structure that was properly described with the standard Powder Diffraction File of pure cubic magnetite (ICDD 75–0449).

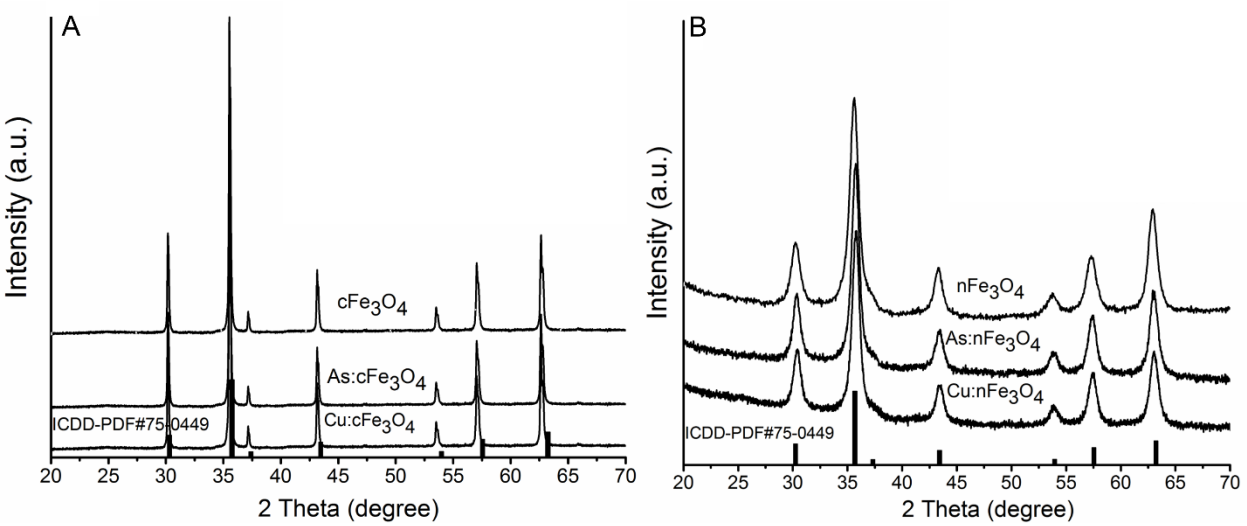

Figure 1: X-ray diffraction patterns of (A): commercial magnetite (cFe_3O_4) before and after As^{3+} ($As:cFe_3O_4$) and Cu^{2+} ($Cu:cFe_3O_4$) adsorption; (B): synthesized magnetite (nFe_3O_4) before and after As^{3+} (As:nFe3O4) and Cu^{2+} ($Cu:nFe_3O_4$) adsorption.

The cFe_3O_4 magnetite showed intense and sharp diffraction peaks attesting a well crystallized structure whereas nFe_3O_4 XRD patterns appeared extremely broad and might underline small particles. The X-ray diffraction pattern of commercial magnetite (cFe_3O_4) and synthesized magnetite (nFe_3O_4) before and after As^{3+} ($As:cFe_3O_4$ and $As:nFe_3O_4$) and Cu^{2+} ($Cu:cFe_3O_4$ and $Cu:nFe_3O_4$) adsorption were compared in Figures 1A-B. As reference, the Powder Diffraction File (PDF) standard cards of pure cubic magnetite (ICDD 75–0449) were represented at the bottom of the figure. The peaks observed in the XRD spectra of cFe_3O_4 and nFe_3O_4 before and after As^{3+} and

Cu^{2+} adsorption were in good agreement with the structural model of ICSD card PDF file number 75-0449 and only the presence of cubic magnetite peaks were remarked. The effect of As^{3+} and Cu^{2+} ions substitutions on the crystal structure of cFe_3O_4 and nFe_3O_4 was evidenced by a variation of the (hkl) peaks positions of the spinel structure of Fe_3O_4 (ICCD card PDF file number 75-0449). The adsorption of As^{3+} and Cu^{2+} ions onto the Fe_3O_4 lattice caused an increment of the a-axes in the unit cell of Fe_3O_4 (Table 1). Rietveld refinement analysis was undertaken for an estimation of the lattice parameters. On the other hand, the quantitative analysis by the Rietveld method of the experimental data was evaluated by the values of the discrepancy factor (R_{wp}), expected weighted profile factor (R_{exp}), Bragg factor (R_{Bragg}) and goodness of fit (χ^2) (http://maud.radiographema.eu/). Values obtained for parameters determined by Rietveld method are in agreement to data presented in the literature (Zakaria et al 2003; Pandit et al., 2003). The values of the calculated parameters are presented in Table 1.

Table 1: Lattice parameters of samples calculated from XRD

Samples	cFe_3O_4	As: cFe_3O_4	Cu: cFe_3O_4	n Fe_3O_4	As: nFe_3O_4	Cu: nFe_3O_4
R_{wp} (%)	8.96	8.78	8.67	8.99	8.12	8.32
R_{exp} (%)	5.98	6.38	6.45	6.05	6.17	6.23
R_{Bragg} (%)	3.4	2.95	2.87	3.05	2.90	2.92
χ^2	1.67	1.89	1.92	1.55	1.71	1.82
a- axes (nm)	8.395	8.397	8.40	8.39	8.392	8.394
D_{XRD} (nm)	85±0.3	80 ± 0.3	76 ± 0.1	12±0.2	10 ± 0.2	9 ± 0.2

The results revealed that the obtained materials were standard Fe_3O_4. The cFe_3O_4 and nFe_3O_4 samples after the adsorption of As^{3+} and Cu^{2+} ions had also a spinel structure. The average particle sizes was determined using Scherrer equation (Cullity, 1956) and are also listed Table 1.

The adsorption and desorption isotherms of nitrogen gas revealed classical features for iron oxides (Figure 2).

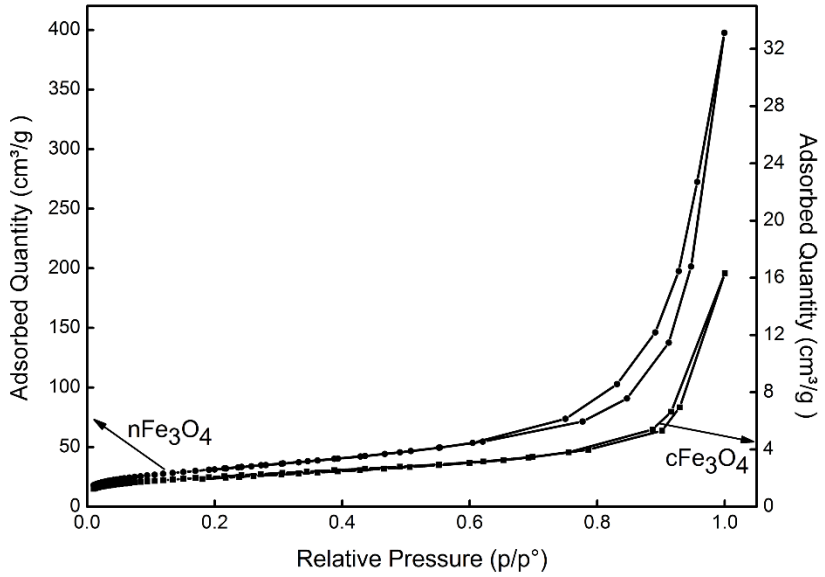

Figure 2: Nitrogen sorption/desorption isotherm of cFe_3O_4 and nFe_3O_4 magnetite samples.

The BET calculation applied to the nitrogen desorption isotherm gave a total specific surface area for the cFe_30_4 of about 6.8 m^2/g, and 100 m^2/g for the synthetized magnetite, nFe_3O_4, that correlated the information obtained by X-Ray diffraction. Indeed, it was not surprising to get a wide specific surface area for nFe_3O_4 that displayed small particles (10 nm) while the commercial magnetite showed bigger particles and thus a smaller specific surface area than the synthesized magnetite prepared here. Moreover, in order to give an information about the accessible surface area which is one the most important parameters that play an important role on the reactivity of the materials for the adsorption of chemical compounds, BET calculation drove to the determination of the pore volume and average pore diameter which were 0.025 cm^3/g and 14.96

nm for cFe_3O_4 and 0.61 cm^3/g and 24.39 nm for nFe_3O_4, respectively. When the size of particles decreased from a D_{nFe3O4}/D_{cFe3O4} ratio of 7 according to the XRD, the BET surface area ratio increased 14.76 times while the pore volume ratio increased 24 times and the average pore diameter ratio increased 1.63 times. The BET data of cFe_3O_4 and nFe_3O_4 changed when the average particle size decreased 7 times, thus leading to an increase in surface/volume ratio of the particles. The morphology of both synthesized and commercial magnetite before and after the adsorption of As^{3+} and Cu^{2+} ions was studied by scanning electron microscopy (Figure 3). In the case of the synthesized magnetite (nFe_3O_4 - Figure 3A), the particles had nanometric sizes and exhibited spherical morphology. Moreover, the morphology of the nFe_3O_4 did not change after the adsorption of As^{3+} and Cu^{2+} ions (Figure 3B and Figure 3C). On the other hand, the commercial magnetite (Figure 3D) particles had irregular shapes and were bigger than the synthesized ones.

As in the case of nFe_3O_4, the morphology of the commercial magnetite particles was not influenced by the adsorption of heavy metal ions. In both cases (synthesized and commercial magnetite), the dimension of the particles decreased after the adsorption experiments. After adsorption experiments the dimension of the nFe_3O_4 (14.7±0.8) particles decreased to 12.6±0.6 ($As:nFe_3O_4$) and 10.8±0.6 nm ($Cu:nFe_3O_4$). For the cFe_3O_4 samples, the dimension of the particles decreased from 91.2±0.8 to 86±0.8 nm ($As:cFe_3O_4$) and 80±0.5 nm ($Cu:cFe_3O_4$).The estimated mean particles sizes were in good agreement with the XRD results.

EDAX spectra of the synthesized and commercial magnetite after the adsorption of As^{3+} and Cu^{2+} ions were acquired (Figure 4). In the case of $As:nFe_3O_4$ and $As:cFe_3O_4$ samples, the EDAX spectra (Figure 3A and Figure 3C) confirmed the presence of the Fe, O and As. Also, the $As:nFe_3O_4$ sample contained a larger quantity of arsenic than the $As:cFe_3O_4$ sample.

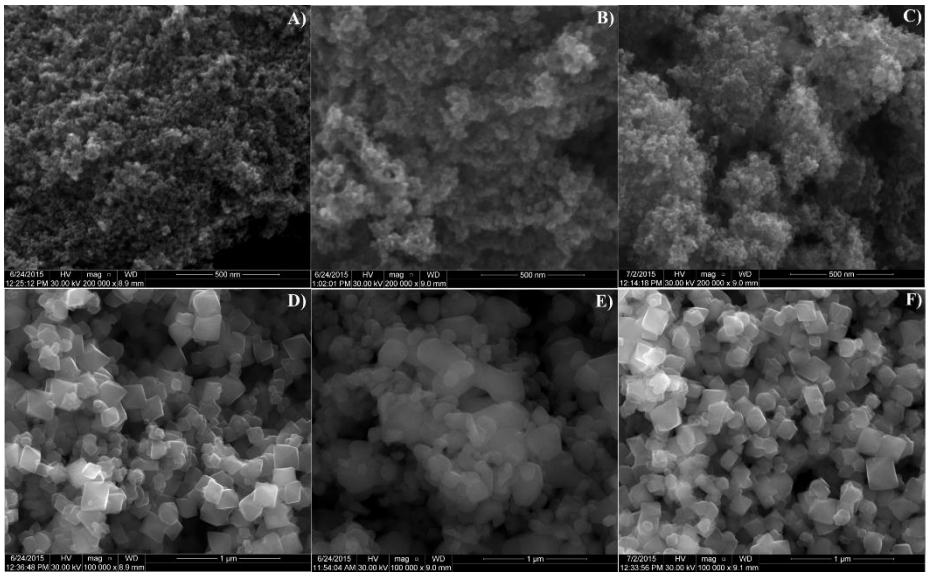

Figure 3. SEM images of nFe_3O_4 (A), $As:nFe_3O_4$ (B), $Cu:nFe_3O_4$ (C), cFe_3O_4 (D), $As:cFe_3O_4$ (E) and $Cu:cFe_3O_4$ (F) samples.

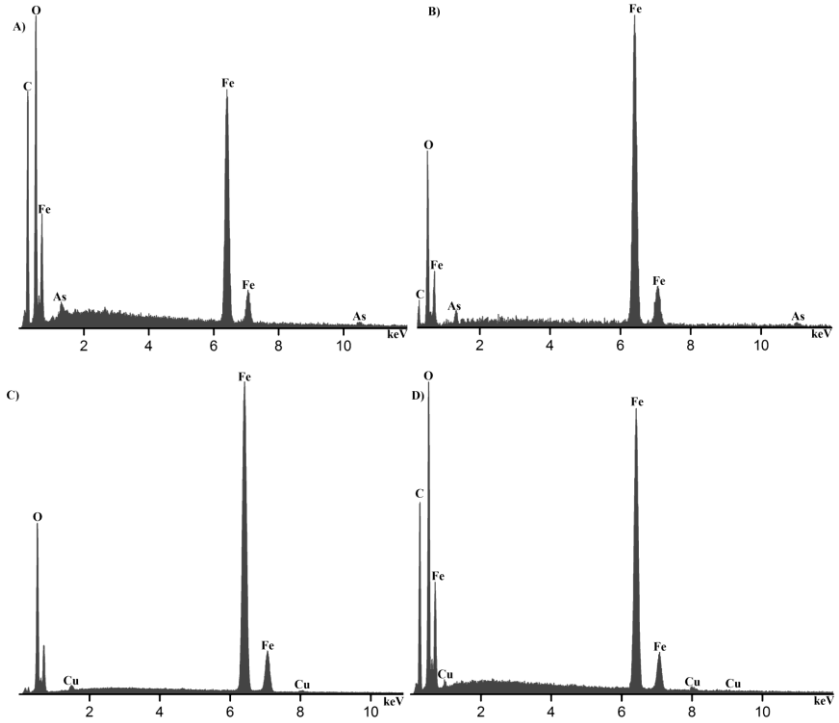

Figure 4. EDAX spectra of $As:nFe_3O_4$ (A), $Cu:nFe_3O_4$ (B), $As:cFe_3O_4$ (C) and $Cu:cFe_3O_4$ (D) powders.

On the other hand, the EDAX spectra of Cu:nFe_3O_4 (Figure 4B) and Cu:cFe_3O_4 (Figure 4D) presented all the constituent elements of the powders (Cu, Fe and O). In this case, both samples (Cu:nFe_3O_4 and Cu:cFe_3O_4) had roughly the same copper content. The As^{3+} and Cu^{2+} immobilized by cFe_3O_4 or nFe_3O_4 powders did not appear to affect the diffraction patterns of Fe_3O_4 but were detected by EDAX analysis. All the elements detected by EDAX are in good agreement with the crystalline phase detected by XRD.

The TEM micrographs were also obtained for the nFe3O4 (Figure 5A) and cFe3O4 (Figure 5B) samples.

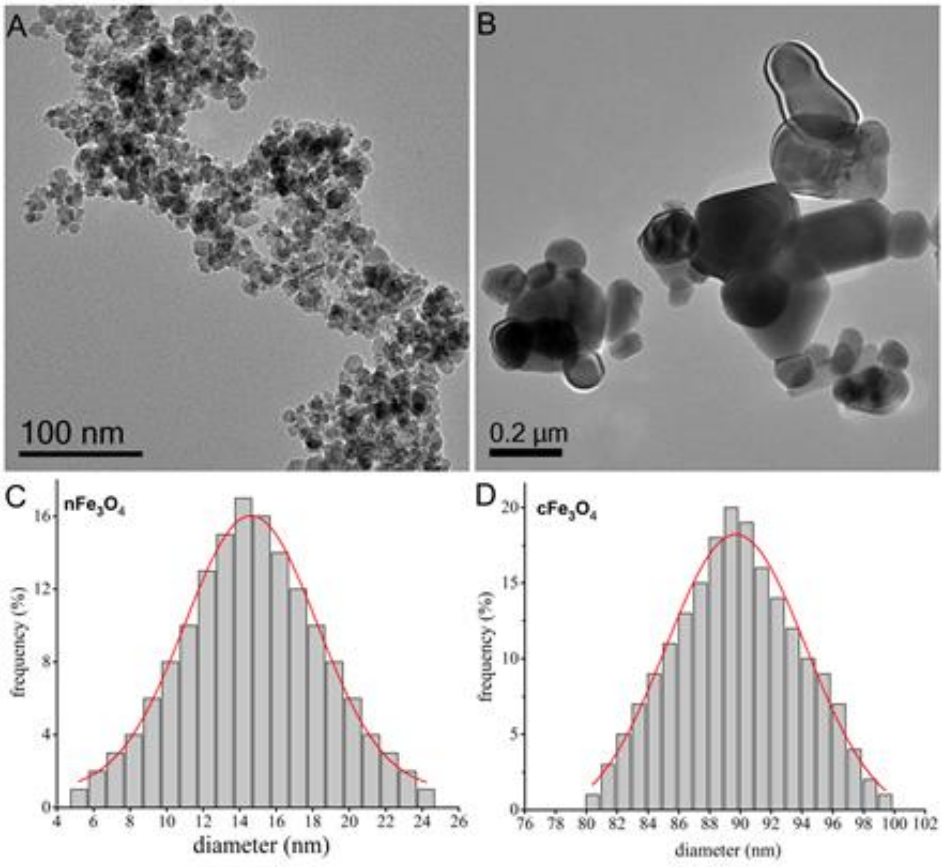

Figure 5: TEM micrographs of nFe_3O_4 (A), cFe_3O_4 (B) samples. The particle size distributions of nFe_3O_4 (C), cFe_3O_4 (D) samples was also determined.

The TEM studies confirmed that the synthesized magnetite samples consist of small, spherical nanoparticles. On the other hand, the particle size distributions (Figure 5C-D) were determined from TEM micrographs. The mean particle size calculated by TEM analysis was 14.2±0.3 nm for nFe_3O_4 and 89.4±0.6 nm for cFe_3O_4, respectively. These results were in good agreement with the XRD and SEM results.

In this study, we compared the diameter of nFe_3O_4 and cFe_3O_4 nanoparticles using XRD, SEM, TEM and DLS methods. XRD, TEM and DLS methods give different information about particle size. For SEM, TEM and XRD analysis the samples must be dried while for DLS analysis the particles are in a suspension state. DLS method is based on the statistical fluctuations of the scattered light due to the Brownian motion of the particles in the control (Lee et al., 2013). The mean particle sizes calculated from XRD, SEM, TEM and DLS for nFe_3O_4 and cFe_3O_4 are presented in Table 2. The mean particle sizes from XRD, SEM, TEM and DLS were called D_{XRD}, D_{SEM}, D_{TEM} and D_{DLS}, respectively. The mean particle sizes obtained from XRD, SEM and TEM methods are comparable while the mean particle sizes obtained from DLS were bigger. This result could be explained by the fact that D_{DLS} were measured in a suspension state. As a result, DDLS gives mean hydrodynamic size which is usually larger than D_{XRD}, D_{SEM} or D_{TEM} as it includes a few solvent layers.

Table 2: Mean particle sizes measured by XRD, SEM, TEM and DLS analysis

Samples	D_{XRD} (nm)	D_{SEM} (nm)	D_{TEM} (nm)	D_{DLS} (nm)
cFe_3O_4	85 (± 0.5)	91.2 (± 0.8)	89.4 (± 0.6)	198 (± 6.3)
nFe_3O_4	12 (± 0.2)	14.7 (± 0.5)	14.2 (± 0.3)	32 (± 3.5)

3.2. Adsorption properties of magnetite nanoparticles for As and Cu removal

Adsorption isotherm models are fundamental for describing the interactive behavior between the adsorbate and adsorbent and are also important for investigating mechanisms of adsorption. In this study, equilibrium data were analyzed using the Freundlich and Langmuir isotherms. The equilibrium adsorption isotherms and the Freundlich and Langmuir isotherm linearized models are shown in Figures 6 and 7. Replicates of the adsorption experiments were run in order to evaluate the experimental reproducibility. The experiments were performed in triplicate and the mean values were considered for the Langmuir isotherm. The standard deviation (SD) for each point of the Langmuir isotherm of the replicates of the uptake of arsenic and copper onto commercial and synthetic magnetic nanoparticles were also presented in Figure 6.

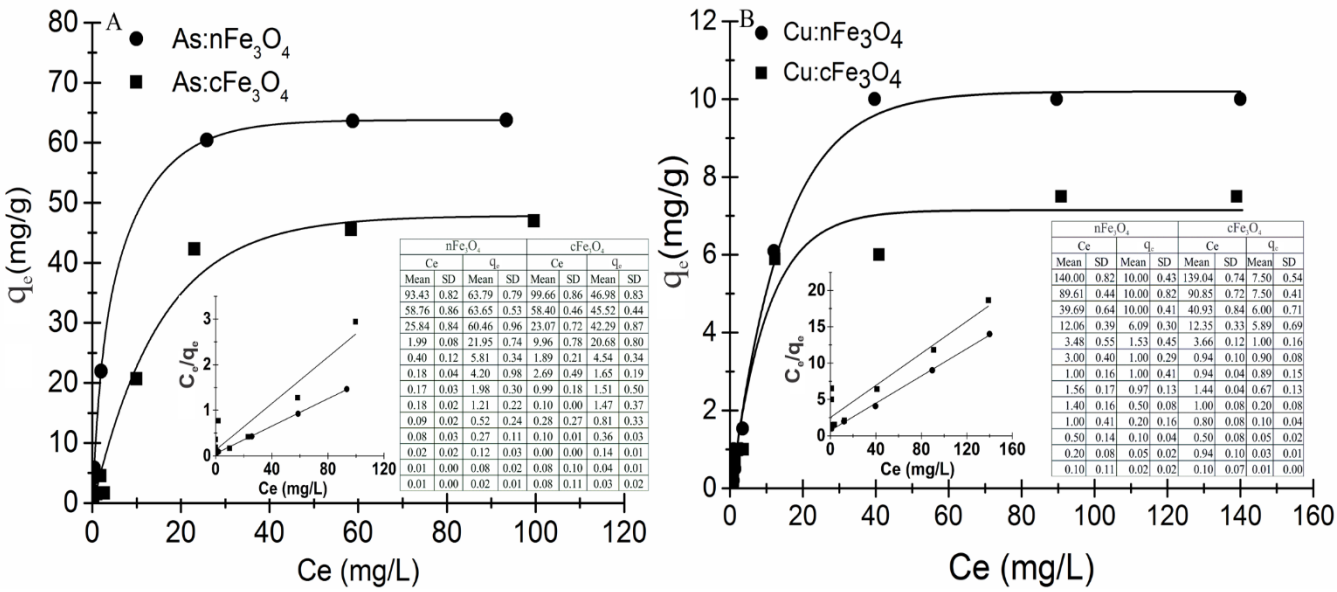

nFe_3O_4				cFe_3O_4			
Ce		q_e		Ce		q_e	
Mean	SD	Mean	SD	Mean	SD	Mean	SD
93.43	0.82	63.79	0.79	99.66	0.86	46.98	0.83
58.76	0.86	63.65	0.53	58.40	0.46	45.52	0.44
25.84	0.84	60.46	0.96	23.07	0.72	42.29	0.87
1.99	0.08	21.95	0.74	9.96	0.78	20.68	0.80
0.40	0.12	5.81	0.34	1.89	0.21	4.54	0.34
0.18	0.04	4.20	0.98	2.69	0.49	1.65	0.19
0.17	0.03	1.98	0.30	0.99	0.18	1.51	0.50
0.18	0.02	1.21	0.22	0.10	0.00	1.47	0.37
0.09	0.02	0.52	0.24	0.28	0.27	0.81	0.33
0.08	0.03	0.27	0.11	0.10	0.01	0.36	0.03
0.02	0.02	0.12	0.03	0.00	0.00	0.14	0.01
0.01	0.00	0.08	0.02	0.08	0.10	0.04	0.01
0.01	0.00	0.02	0.01	0.08	0.11	0.03	0.02

nFe_3O_4				cFe_3O_4			
Ce		q_e		Ce		q_e	
Mean	SD	Mean	SD	Mean	SD	Mean	SD
140.00	0.82	10.00	0.43	139.04	0.74	7.50	0.54
89.61	0.44	10.00	0.82	90.85	0.72	7.50	0.41
39.69	0.64	10.00	0.41	40.93	0.84	6.00	0.71
12.06	0.39	6.09	0.30	12.35	0.33	5.89	0.69
3.48	0.55	1.53	0.45	3.66	0.12	1.00	0.16
3.00	0.40	1.00	0.29	0.94	0.10	0.90	0.08
1.00	0.16	1.00	0.41	0.94	0.04	0.89	0.15
1.56	0.17	0.97	0.13	1.44	0.04	0.67	0.13
1.40	0.16	0.50	0.08	1.00	0.08	0.20	0.08
1.00	0.41	0.20	0.16	0.80	0.08	0.10	0.04
0.50	0.14	0.10	0.04	0.50	0.08	0.05	0.02
0.20	0.08	0.05	0.02	0.94	0.10	0.03	0.01
0.10	0.11	0.02	0.02	0.10	0.07	0.01	0.00

Figure 6: Equilibrium adsorption isotherms for arsenic (A) and copper (B) onto nFe_3O_4 and cFe_3O_4 at room temperature. The inserts highlight the linearized Langmuir fit. Mean and SD values for C_e and q_e are also presented in the inserted tables.

The Langmuir model is based on the assumption of monolayer adsorption on a structurally homogeneous adsorbent, where all sorption sites are identical and energetically equivalent (Suzuki, 1990). The linear form of the Langmuir equation can be expressed according to Eq. (1):

$$\frac{C_e}{q_e} = \frac{C_e}{q_m} + \frac{1}{K_L \times q_m} \quad (1)$$

where q_m is the theoretical maximum adsorption capacity corresponding to monolayer coverage (mg/g), and k_L is the Langmuir constant (L/mg). The k_L and q_m were determined from the linear and angular coefficients of the equations formed by regressing C_e/q_e as a function of C_e. The empirical Freundlich equation is applicable to adsorption on heterogeneous surfaces, where the interaction between the adsorbed molecules is not limited to the formation of a monolayer. The Freundlich constant (k_F) is related to the adsorption capacity of the adsorbent: the higher the value, the greater the affinity for the adsorbate. The empirical parameter 1/n is related to the strength of adsorption, which varies with the heterogeneity of the material. When the values of 1/n are between 0.1 and 1.0, the adsorption process is considered favorable (Liu et al., 2011). The linearized form of the Freundlich equation is expressed according to Eq. (2):

$$lnq_e = lnK_F + \frac{1}{n} lnC_e \quad (2)$$

where k_F is the Freundlich constant (L/g) and 1/n is a dimensionless empirical parameter. The k_F and 1/n values were determined from the linear and angular coefficients of the equations formed by regressing ln q_e as a function of ln C_e, respectively.

To determine whether the adsorption process is favorable, a dimensionless constant separation factor R_L was defined. The adsorption process is irreversible when R_L is zero, favorable

when R_L is between zero and 1.0, linear when R_L is equal to 1.0, and unfavorable when R_L is greater than 1.0. The R_L parameter can be defined based on Eq. (3):

$$R_L = \frac{1}{1+K_L C_0} \quad (3)$$

where C_0 is the initial metal ion concentration (mg/L).

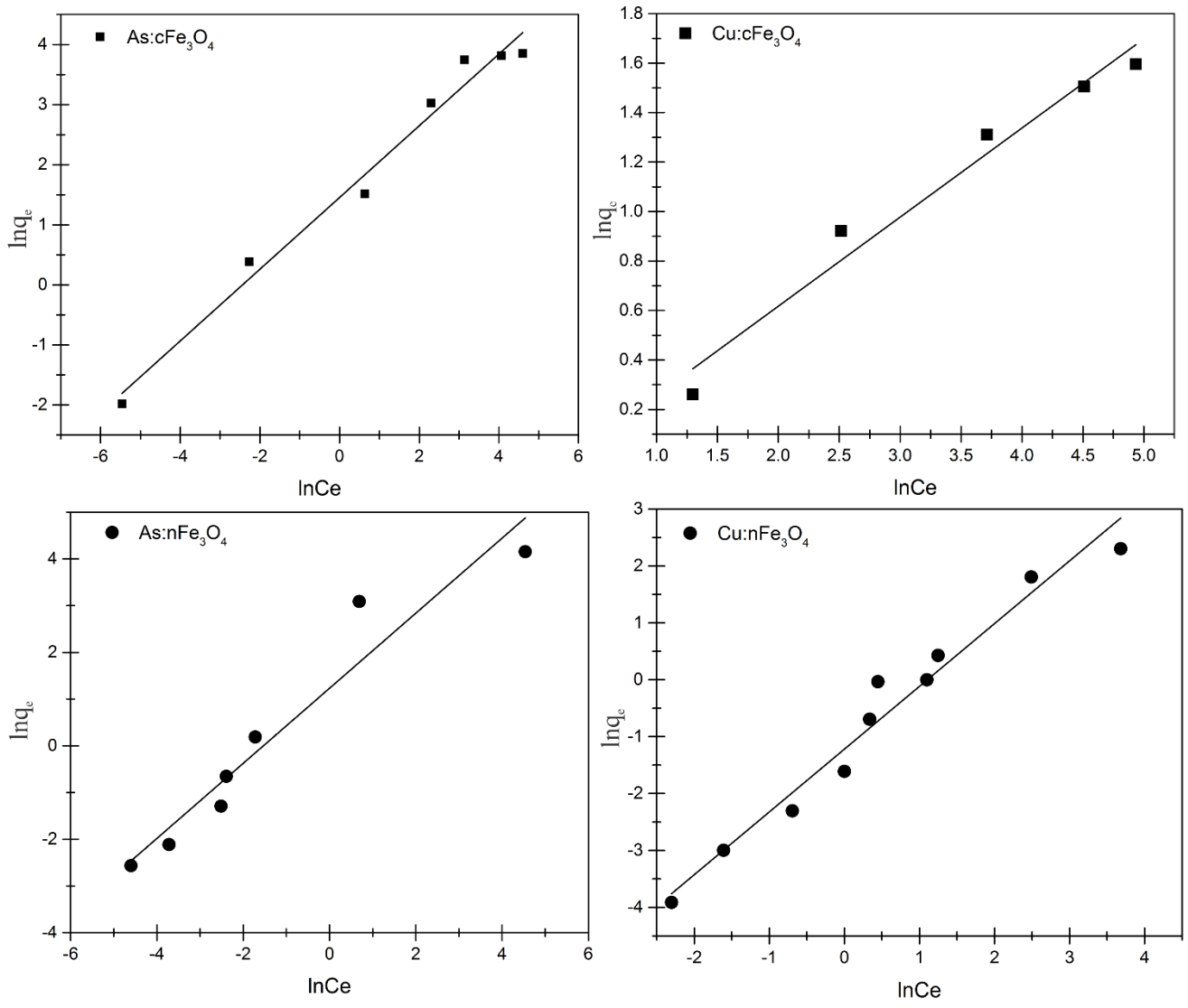

Figure 7: Freundlich linearized fits for the adsorption of both As and Cu onto cFe_3O_4 and nFe_3O_4 magnetite samples.

The isotherm parameters for both As and Cu adsorption by the magnetite were shown in Table 3. As shown, the experimental data were well adjusted to the Langmuir model, once its correlation coefficient (r) was higher that the Freundlich ones. The R_L values were between 0.048-0.734, confirming that the adsorption process was favorable by Langmuir isotherm model. Thus, this data suggested that adsorption mechanism mainly occurred by a monolayer coverage.

Table 3: Parameters derived from both Langmuir and Freundlich fitting models for arsenic and copper adsorption on nFe_3O_4 and cFe_3O_4.

		Langmuir				Freundlich		
		q_m (mg/g)	K_L (L/mg)	R^2	R_L	n	k_f	R^2
As (III)	nFe_3O_4	66.53	0.297	0.999	0.048	1.24	4.37	0.877
	cFe_3O_4	39.26	0.2	0.887	0.113	1.56	2.77	0.896
Cu (II)	nFe_3O_4	10.67	0.13	0.998	0.419	0.9	0.3	0.962
	cFe_3O_4	9.06	0.04	0.871	0.734	2.78	0.9	0.958

The density of the As and Cu was approximately 5.75 and 8.93 g/cm^3 respectively, which yielded an apparent packing area per cations of 0.0415 and 0.0547 nm^2. The specific surface area was determined to reach about 7 and 100 m^2/g for cFe_3O_4 and nFe_3O_4 magnetite samples. If we assumed that those specific surfaces are totally accessible, the calculated amount of adsorbed As cations was 20 and 293 mg/g for cFe_3O_4 and nFe_3O_4 magnetite samples whereas it represented for adsorbed Cu cations almost 13 and 192 mg/g for cFe_3O_4 and nFe_3O_4 magnetite samples. Those maximum adsorbed amounts represented the highest dense covering in a monolayer arrangement

onto the external surface of the magnetite. Here, the maximum adsorption capacity for the solid phase, q_m, estimated through the Langmuir fitting procedure, reached almost 100 and 20% of the whole accessible surface area of cFe_3O_4 and nFe_3O_4 magnetite samples for the adsorption of As^{3+}, and 50 and 5% for the sorption of Cu^{2+}.

The results obtained in our study regarding the adsorption capacity of Cu on cFe_3O_4 and nFe_3O_4 magnetite samples are in good agreement with other similar studies (Huang et al., 2009; Mehdinia et al., 2015). The comparative results showed that the removal efficiencies of the investigated adsorbents were comparable or higher, in some cases. Moreover, Chuang et al. (2005) reported that for chitosan-bound Fe_3O_4 magnetic nanoparticles the adsorption behavior followed the Langmuir adsorption isotherm with a maximum adsorption capacity of 21.5 mg/g. These reported studies are in good agreement with our results and were given as possible explanation for the complexation capability (donor-acceptor interaction) between the surface of the adsorbent and the metal ions (Mehdinia et al., 2015). Also, a study conducted by Mayo et al. (2007) regarding the influence of the magnetite particle size on the arsenic adsorption capacity revealed that the adsorption capacity for As(III) increased with the decrease of the Fe_3O_4 particle size. Mayo et al. (2007) reported an arsenic removal efficiency of 99.2% in the case of 12 nm Fe_3O_4 particles, 90.9% in the case of 20 nm Fe_3O_4 particles and only 24.9% in the case of 300 nm Fe_3O_4 particles. These results were attributed to the increase of the Fe_3O_4 surface area with the decrease of the particle size. Our findings regarding the correlation between the particle size, surface area and arsenic removal efficiency proved to be in agreement with other reported studies. More than that, in agreement with other related studies the higher adsorption capacity for arsenic ions obtained for nFe_3O_4 was attributed to the high specific surface area of these nanoparticles (Mayo et al., 2007; Shipley et al., 2009; Singh et al., 2011). The difference between the adsorption capacity of As and

Cu ions by the two magnetite samples could be attributed to the fact that magnetite has been reported to have a higher affinity towards arsenic compared to copper (Mayo et al., 2007; Shipley et al., 2009; Singh et al., 2011).

On the other hand, recent studies emphasized that the metal removal efficiency of a material can be explained on the basis of surface functionality, competitive affinity of metal ions towards the material used as sorbent, amount of surface charge and availability of active surface sites of the sorbent (Singh et al., 2011; Mondal et al., 2008;). More of that, the metal removal efficiency has proven to be strongly dependent on the size of sorbents (Mayo et al., 2007). Important roles are also played by the batch experiments conditions (pH, sample volume, temperature, adsorbent dosage, initial metal ion concentration, contact time).

With such covering of the surface by adsorbed TE, FTIR spectroscopy measurements were undertaken as a probe to characterize the functional groups of the magnetite samples that were involved for the adsorption (Figure 8).

The main absorption bands found in the synthesized magnetite powders designated the chemical bonds formed between the constituent elements. In this context, the band at 531 cm^{-1} was associated to the Fe-O vibration characteristic to the magnetite phase (Mahdavi et al., 2013a; Mahdavi et al., 2013b). This was the main band from all the spectra. In the case of synthesized magnetite, this band shifted slightly after the adsorption of metal ions from 531 cm^{-1} (nFe_3O_4) to 535 cm^{-1} (As:nFe3O4) and 540 cm^{-1} ($Cu:nFe_3O_4$). The same behavior was noticed in the spectra of the three samples containing commercial magnetite. The band from 531 cm^{-1} (cFe_3O_4) shifted after the adsorption of arsenic ions to 534 cm^{-1} ($As:nFe_3O_4$) and to 538 cm^{-1} after the adsorption of copper ions ($Cu:nFe_3O_4$). Additional peaks in the spectra of the three samples containing synthesized magnetite were found.

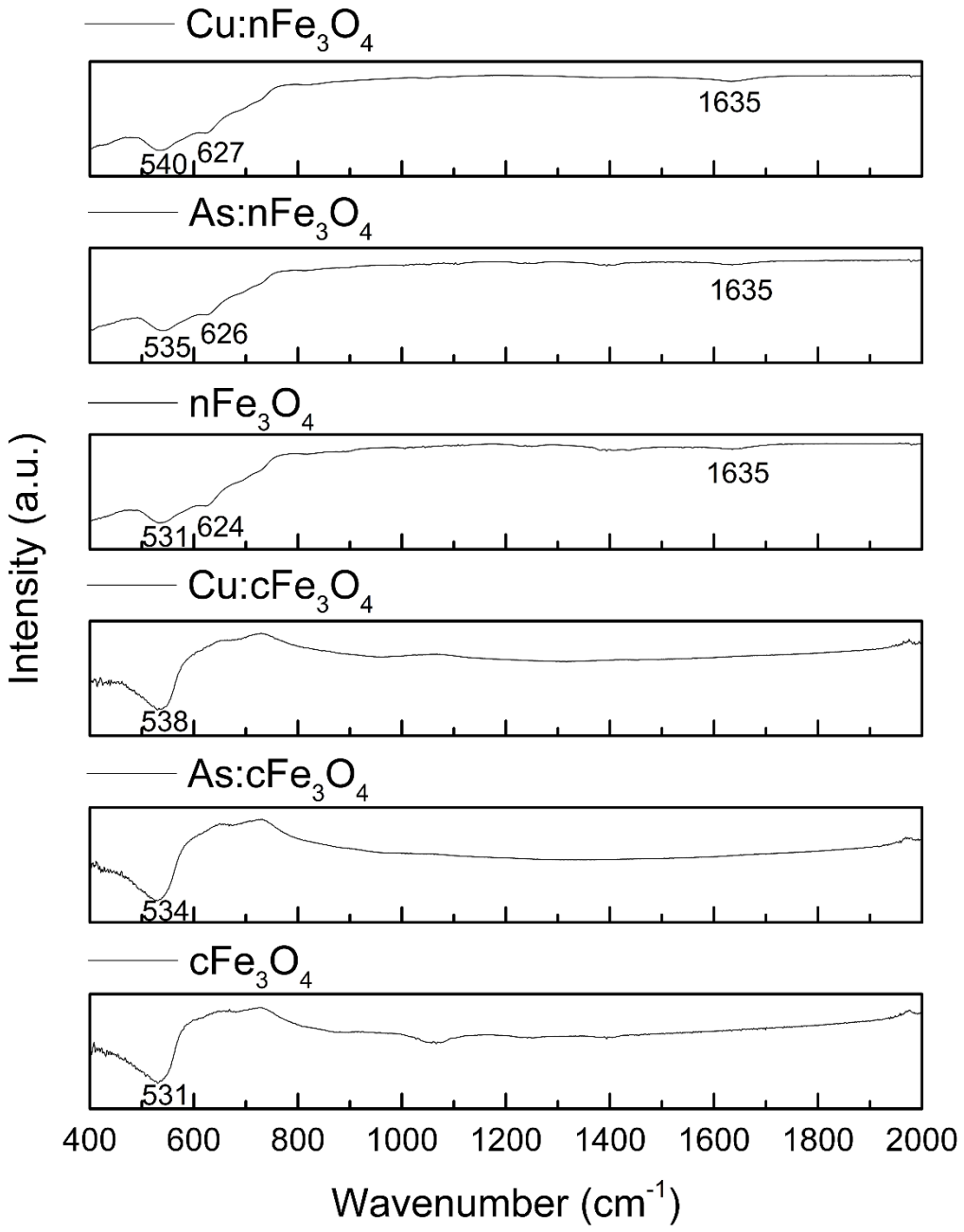

Figure 8: FTIR spectra of both the commercial and synthesized magnetite before (c,nFe_3O_4) and after the adsorption of As ions (As: c,nFe_3O_4) and Cu ions (Cu: c,nFe_3O_4).

Therefore, the band from 624 cm^{-1} (nFe_3O_4), assigned to the Fe-O bond (Khatiri et al., 2012), shifted to 626 cm^{-1} in the spectrum of the sample that adsorbed arsenic ions (As:nFe_3O_4) and to 627 cm^{-1} in the spectrum of the sample that adsorbed copper ions from aqueous media

(Cu:nFe_3O_4). Lastly, the band from 1635 cm^{-1} (Figure 6 A) suggested the presence of hydroxyl groups which most likely appeared on the surface of Fe_3O_4 nanoparticles during their synthesis (Liu et al., 2004; Schwertmann and Cornell, 2003; Yang et al., 2010). This vibrational band was not influenced by the presence of As or Cu ions in the structure of the studied samples.

Additional information on the functional groups from the studied samples were obtained using Raman spectroscopy (Figure 9). The three spectra of the synthesized magnetite before (nFe_3O_4) and after the adsorption of As ions (As:nFe_3O_4) and Cu ions (Cu:nFe_3O_4) (Figure 9A), as well as the three spectra of the commercial magnetite before (cFe_3O_4) and after the adsorption of As ion (As:cFe_3O_4) and Cu ions (Cu:cFe_3O_4) (Figure 9B) were acquired.

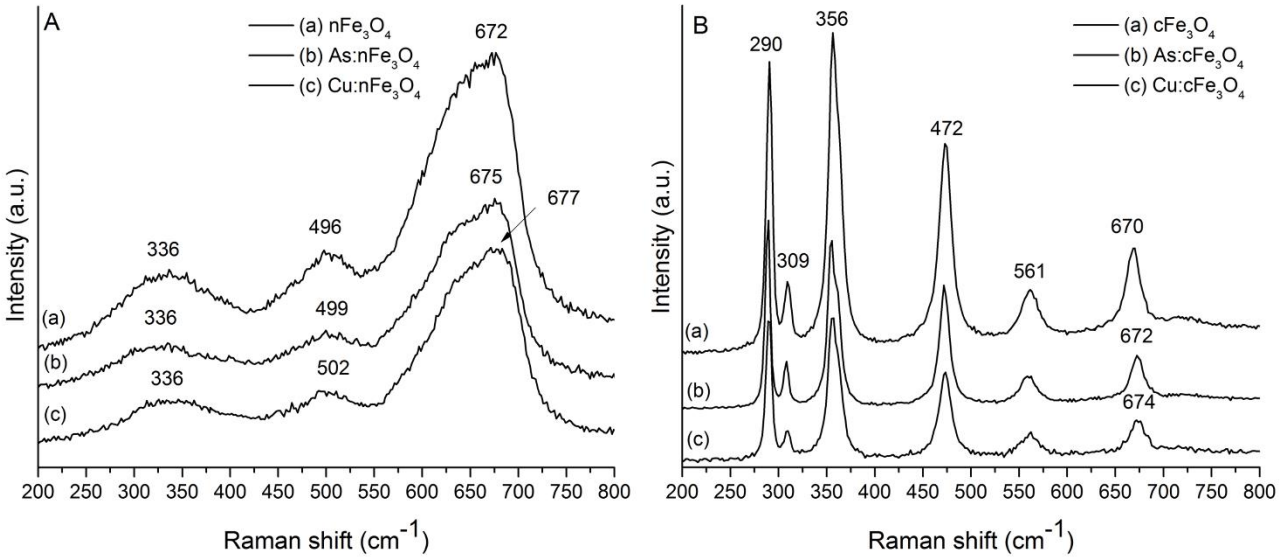

Figure 9: Raman spectra of the synthesized magnetite (A) before (nFe_3O_4) and after the adsorption of As ions (As: nFe_3O_4) and Cu ions (Cu: nFe_3O_4) as well as the spectra of the commercial magnetite (B) before (cFe_3O_4) and after the adsorption of As ions (As: cFe_3O_4) and Cu ions (Cu: cFe_3O_4).

The whole spectra display peaks that are characteristics to magnetite structure. The main feature of the synthesized magnetic (nFe_3O_4) prepared in this study was the enlargement of the Raman bands compared to those of the commercial one. As it has been shown by both XRD and SEM results, such enlargement was related to the size of the nanoparticles which showed a high reactivity to TE. In this context, the peaks found between 250 and 400 cm^{-1} in the spectra of the commercial magnetite (Figure 9B) corresponded to the peak from 336 cm^{-1} from the spectra of synthesized magnetite (Figure 9A) resulting to an overlapping of several peaks. The same conclusion was drawn for the two peaks between 450 and 600 cm^{-1}, which in the case of synthesized magnetite, widened, overlapped and formed the peak from around 490 cm^{-1} (Figure 9A).

The influence of the adsorption of the two ions was evidenced by the shifts of some of the peaks. Indeed, the main peak, which appeared at around 670 cm^{-1} in all the registered spectra was assigned to the A_{1g} mode, characteristic to the magnetite structure (Jubb and Allen, 2010). In the case of synthesized magnetite, this peak shifted slightly from 672 cm^{-1} (nFe_3O_4) to 675 cm^{-1} ($As:nFe_3O_4$) and to 677 cm^{-1} ($Cu:nFe_3O_4$). Also, in the case of commercial magnetite, the band from 670 cm^{-1} shifted after the adsorption As ions to 672 cm^{-1} and after the adsorption of Cu ions to 674 cm^{-1}. Furthermore, the large peak from around 490 cm^{-1} observed in the three spectra of the synthesized magnetite which was assigned to the T_{2g} vibrational mode (Graves et al., 1988; Shebanova and Lazor, 2003) appeared to shift as well after the adsorption of the two heavy metal ions. From 496 cm^{-1} (nFe_3O_4) it shifted to 499 cm^{-1} ($As:nFe_3O_4$) and to 502 cm^{-1} ($Cu:nFe_3O_4$). The same tendency was observed in the FTIR spectra, in the case of the peaks characteristic to the magnetite phase. The third peak from the spectra of synthesized magnetite (Figure 9A), from 336

cm^{-1}, was assigned to the E_g vibrational mode characteristic to the Fe_3O_4 structure (Graves et al., 1988; Shebanova and Lazor, 2003).

One of the most important environmental problems for which solutions are sought, is the removal of toxic contaminants from waters. Due to their toxicity and non-biodegradable nature, the presence of heavy metals in surface water represents a serious environmental and public health problem. For removing trace metals from waters, researchers established that adsorption is an alternative method economically feasible. Unfortunately, cationic and anionic adsorption on oxide surfaces is not well enough understood and continues to be extensively studied. Moreover, establishing adsorption models is difficult enough due to the fact that it must take into account numerous parameters. However, the adsorption process modeling is currently a widely studied topic because they could allow assessment of heavy metals in natural environments and also design adsorption treatment units used to remove contaminants from contaminated waters. Previous studies (Anderson et al., 1976) demonstrated that anions and cations are capable of distinctive adsorption onto oxide surfaces and the adsorption of anions and cations sontrgly depends on the pH. Thereby, cations can be adsorbed onto positively charged surfaces while anions can be adsorbed onto negatively charged surfaces. Previous studies conducted by Hingston el al. **Hingston et al., 1972**) established that adsorption of weak acid anions on any oxide surface decreases as the pH increases. James and Healy (**James and Healy, 1972**) showed that the adsorption of cobalt ions decreases when the pH decreases. On the assumption that the adsorption is controlled by microcrystalline surface growth, Hsu and Rennie (Hsu and Rennie, 1962**)** proposed a mechanism for anion adsorption on soil adsorbents. Stumm and Bilinsk (Stumm and Bilinski, 1972) demonstrated that the adsorption of metal ions at the solid-solution interface is governed by the much stronger adsorbed hydroxo, sulfato, carbonato and other metal species according to:

$$MM_{aq}^{Z+} + nH_2O \leftrightharpoons M(OH)_n^{(Z-n)} + nH^+ \quad (4)$$

In addition, the key reason for the enhanced removal seems to be the presence of hydroxide ions. The presence of hydroxyl ions could lead to easier adsorption of copper or arsenic ions on the surface lattice which follows further adsorption. It is known that (Elliott and Huang, 1981) an important means for controlling the extent of pollution due to liquid waste or sewage discharged into a river or the sea is the adsorption at solid-solution interface. On the other hand, previous studies (Panday et al., 1985) showed that the removal of pollutants from wastewaters by adsorption is highly dependent on the pH of the solution which affects the surface charge of the adsorbent, the degree of ionization and the speciation of adsorbate.

4. Conclusions

Ferrous chloride tetrahydrate and ferric chloride hexahydrate were used as precursors in a co-precipitation method at room temperature, in a controlled atmosphere, for the synthesis of magnetite nanoparticles (~12 nm). The synthesized particles had a magnetite crystal structure with a grain size of around 12 (± 0.2) nm. The BET surface area and average pore size of the synthesized magnetite (nFe_3O_4) nanoparticles were 100.5179 m^2/g and 24.39779 nm. On the other hand, the BET surface area and average pore size of the commercial Fe_3O_4 particles were 6.8075 m^2/g and 14.96434 nm, respectively. The adsorption isotherms of As and Cu onto synthesized magnetite and commercial magnetite particles were obtained under relevant conditions. The adsorption of As and Cu was described by a Langmuir type isotherm. A good Langmuir fit for the adsorption isotherms of As was obtained. The coefficient of Langmuir isotherm (R^2) at room temperature was 0.999 for synthesized magnetite and 0.886 for the commercial magnetite. In this case, the maximum adsorption capacity for the solid phase (q_m) was 66.53 mg/g for synthesized magnetite and 39.24 mg/g for commercial magnetite. On the other hand, the Langmuir constant K_L was 0.297

for synthesized magnetite and 0.2 for commercial magnetite. The combination of a high specific area and due to the possibility of being magnetically separated, the developed magnetic iron oxide nanoparticles in this study are revealed to be a good material for the depollution of drinking water or for the removal of toxic elements like heavy metals from contaminated waters and/or soils.

Acknowledgements:

The work has been funded by the PICS/2014 Project" Nanoengineered particles for contaminated sites remediation (NANOREMEDIATION)".

References

Anderson, M.A., Ferguson J.F., Gavis, J., 1976. Arsenate Adsorption On Amorphous Aluminum Hydroxide. J. Colloid Interface Sci. 54, 391-399.

Barbuceanu, F., Diaconua, C. Stamate, D. Raita, S., Popovici, A., Georgescu, B., Belu, C., Predoi, G., 2015.Histopathological Study Of Brain From Cattle With Nervous Symptomatology, Agric. Agric. Sci. Procedia 6, 287 – 292.

Bonetto L.R., Ferrarini F., de Marco C., Crespo J.S., Guégan R. and Giovanela M. 2015 Removal of methyl violet 2B dye from aqueous solution using a magnetic composite as an adsorbent. Journal of Water Process Engineering, 6, 11-20.

Brown, Jr., G.E., Parks, G.A., 2001. Sorption of trace elements on mineral surfaces: modern perspectives from spectroscopic studies, and comments on sorption in the marine environment. Int. Geol. Rev. 43, 963–1073.

Brunauer, S., Emmett, P. H., Teller, E., 1938. Adsorption of Gases in Multimolecular Layers. J. Am. Chem. Soc. 60, 309–319.

Chang, Y.-C., Chen D.-H., 2005. Preparation and adsorption properties of monodisperse chitosan-bound Fe3O4 magnetic nanoparticles for removal of Cu(II) ions. J. Colloid. Interface. Sci .283, 446–451.

Cho, D.-W., Jeon, B.-H., Chon, C.-M., Kim, Y., Schwartz, F.W., Lee, E.-S., Song, H., 2012. A novel chitosan/clay/magnetite composite for adsorption of Cu(II) and As(V). Chem. Eng. J. 200–202, 654–662.

Cullity, B.D., 1956. Elements of X-ray Diffraction . Addision-Wesley Publishing COmpany.

Dalida, M.L.P., Mariano, A.F.V., Futalan, C.M., Kan, C.-C., Tsai, W.-C., Wan, M.-W., 2011. Adsorptive removal of Cu(II) from aqueous solutions using non-crosslinked and crosslinked chitosan-coated bentonite beads. Desalination 275, 154–159.

Elliott, H.A., Huang, C. P., 1981. Adsorption characteristics of some Cu(ll) complexes on alumino silicates, Water Res. 15, 849.

Ferguson, J.F., Gavis J., (Eds), 1972. A Review Of The Arsenic Cycle In Natural Waters. Water Research Pergamon Press. Vol. 6, pp. 1259-1274. Printed in Great Britain.

Gilbert, B., Banfield, J.F., 2005. Molecular-scale processes involving nanoparticulate minerals in biogeochemical systems. Rev. Mineral. Geochem. 59, 109–155.

Gómez-Pastora, J., Bringas, E., Ortiz, I., 2014. Recent progress and future challenges on the use of high performance magnetic nano-adsorbents in environmental applications. Chem. Eng. J. 256,187–204.

Graves, P.R., Johnston, C., Campaniello, J.J., 1988. Raman scattering in spinel structure ferrites. Mater. Res. Bull. 23, 1651–1660.

Guégan, R. Giovanela, M. Motelica-Heino, M. ‘Nonionic organoclay: a ‘swiss army knife’ for the adsorption of micro-pollutants?’ J. Colloid Interface Sci., 437 (1) 71-79 (2015).

Harikishore, D., Reddy, K., Yun, Y.-S., 2016. Spinel ferrite magnetic adsorbents: Alternative future materials for water purification?. Coord. Chem. Rev. 315, 90–111.

He, J., Charlet, L., 2013. A review of arsenic presence in China drinking water. J. Hydrol. 492, 79–88, doi:http://dx.doi.org/10.1016/j.jhydrol.2013.04.007.

Hingston, F.J., Posner, A. M., Quirk, J.P., 1972. Anion Adsorption by goethite and gibbsite I. The role of the proton in determining adsorption envelopes. J. Soil Sci. 23, 177-192.

Hochella, Jr., M.F., Moore, J.N., Putnis, C.V., Putnis, A., Kasama, T., Eberl, D.D., 2005. Direct observation of heavy metal–mineral association from the Clark Fork River Superfund Complex: implications for metal transport and bioavailability. Geochim. Cosmochim. Acta 69, 1651–1663.

Hsu, P. H. and Rennie, D. A., 1962. Reactions of phosphate in aluminum system. 1. Adsoprtion of phosphate by X-Ray amorphous aluminum hydroxide. Can. J. Soil. Sci. 42, 197-209.

Huang, S.-H., Chen D.-H., 2009. Rapid removal of heavy metal cations and anions from aqueous solutions by an amino-functionalized magnetic nano-adsorbent J. Hazard. Mater. 163, 174–179.

James, R. O., and Healy, T.W., 1972. Adsorption Of Hydrolysable Metal Ions At The Oxide Water Interface I. Co(Ii) Adsorption On Sio2 And Tio2 As Model Systems. J. Colloid Interface Sci. 40, 42-52.

Jubb A.M., Allen, H.C., 2010. Vibrational spectroscopic characterization of hematite, maghemite, and magnetite thin films produced by vapor deposition. ACS Appl. Mater. Interfaces, 2, 2804–2812.

Kanel, S.R., Greneche, J-M. Choi, H, 2006. Arsenic(V) Removal from Groundwater Using Nano Scale Zero-Valent Iron as a Colloidal Reactive Barrier Material Environ. Sci. Technol. 40, 2045-2050.

Kartinen, E.O., Martin, C.J., 1995. An overview of arsenic removal processes. Desalination 103, 79–88, doi:http://dx.doi.org/10.1016/0011-9164 (95) 00089-5.

Khatiri, R., Reyhani, A., Mortazavi, S.Z., Hossainalipour, M., 2012. Preparation and characterization of Fe_3O_4/SiO_2/APTES core-shell nanoparticles. Proceedings of the 4th International Conference on Nanostructures (ICNS4) 12-14 March, Kish Island, I.R. Iran.

Langmuir, I., 1918. The adsorption of gases on plane surfaces of glass, mica and platinum. J. Am. Chem. Soc. 40, 1361–1403.

Lee, D.-H., Cho, G.S., Lim, H.M., Kim, D.S., Kim, C., Lee S.H., 2013. Comparisons of particle size measurement method for colloidal silica. J. Ceram. Process. Res. 14, 274-278.

Liu R., Zhang B., Mei D., Zhang H. and Liu J. 2011 Adsorption of methyl violet from aqueous solution by halloysite nanotubes. Desalination, 268, 111-116.

Liu, X.Q., Ma, Z.Y., Xing, J.M., Liu, H., 2004. Preparation and characterization of amino-silane modified superparamagnetic silica. Nanospheres. J. Magn. Magn. Mater. 270, 1–6.

Lunge, S., Singh, S., Sinha, A., 2014. Magnetic iron oxide (Fe_3O_4) nanoparticles from tea waste for arsenic removal. J. Magn. Magn. Mater. 356, 21–31.

Mahdavi, M, Ahmad, M.B., Haron, M.J., Namvar, F., Nadi, B., Ab Rahman M.Z., Amin, J., 2013, a. Synthesis, Surface Modification and Characterisation of Biocompatible Magnetic Iron Oxide Nanoparticles for Biomedical Applications. Molecules 18, 7533-7548

Mahdavi, M., Ahmad, M.B., Haron, M.J., Gharayebi, Y., Shameli, K., Nadi, B., 2013,b. Fabrication and characterization of SiO_2/(3-Aminopropyl) triethoxysilane-coated magnetite nanoparticles for Lead(II) removal from aqueous solution. J. Inorg. Organomet. Polym. 23, 599–607.

Massart, R., 1979. Magnetic fluids and process for obtaining them. French Patent, 79, 18842.

Massart, R., 1982. Magnetic fluids and process for obtaining them. U.S. Patent 4(329), 241

Mayo, J.T., Yavuz, C., Yean, S., Cong, L., Sipley, H., Yu, W., Falkner, J., Kan, A., Tomson, M., Colvin, V.L., 2007. The effect of nanocrystalline magnetite size on arsenic removal, Sci. Technol. Adv. Mater. 8, 71–75.

Mehdinia, A., Shegefti, S., Shemirani, F., 2015. Removal of Lead(II), Copper(II) and Zinc(II) Ions from Aqueous Solutions Using Magnetic Amine-Functionalized Mesoporous Silica Nanocomposites. J. Braz. Chem. Soc. 26, 2249-2257.

Mehta, D., Mazumdar, S., Singh, S.K., 2015. Magnetic adsorbents for the treatment of water/wastewater—A review. J. Wat. Proc.Eng. 7, 244–265.

Mondal, P., Majumder, C.B., Mohanty B., 2008. Effects of adsorbent dose, its particle size and initial arsenic concentration on the removal of arsenic, iron and manganese from simulated ground water by Fe^{3+} impregnated activated carbon. J. Hazard. Mater. 150, 695–702.

Panday, K.K., Prasad, G., Singh, V. N., 1985. Copper(II) Removal From Aqueous Solutions By Fly Ash. Water Res. 19, 869-873.

Pandit, A.A., More, S.S., Dorik, R.G., Jadhav, K.M., 2003. Structural and magnetic properties of Co1+ySnyFe2-2y-xCrxO4 ferrite system. Bull. Mater. Sci.26, 517–521.

Pontius, F.W., Brown, K.G., Chen, C.J., 1994. Health implications of arsenic in drinking. J. Am. Water Works Assoc. 86, 52–63.

Predoi, D., 2007. A study on iron oxide nanoparticles coated with dextrin obtained by coprecipitation. Dig. J. Nanomater. Bios. 2, 169-173.

Savage, N., Diallo, M.S., 2005. Nanomaterials and water purification: opportunities and challenges, J. Nanopart. Res. 7, 331–342.

Schwertmann, U., Cornell, R.M., 2003. The Iron Oxide: Structure, Properties, Reactions, Occurrence and Uses, second ed., Wiley–VCH, Denmark.

Shebanova O.N., Lazor, P., 2003. Raman spectroscopic study of magnetite ($FeFe_2O_4$): a new assignment for the vibrational spectrum. J. Solid State Chem. 174, 424–430.

Shipley, H.J., Yean, S., Kan, A.T., Tomson, M.B., 2009. Adsorption Of Arsenic To Magnetite Nanoparticles: Effect Of Particle Concentration, Ph, Ionic Strength, And Temperature. Environ. Toxicol. Chem. 28, 509–515.

Simeonidis, K., Gkinis, T., Tresintsi, S., Martinez-Boubeta, C., Vourlias, G., Tsiaoussis, I., Stavropoulos, G., Mitrakas, M., Angelakeris, M., 2011. Magnetic separation of hematite-coated Fe3O4 particles used as arsenic adsorbents. Chem. Eng. J. 168, 1008-1015.

Singh, S., Barick, K.C., Bahadur D., 2011. Surface engineered magnetic nanoparticles for removal of toxic metal ions and bacterial pathogens. J. Hazard. Mater. 192, 1539– 1547.

Sivashankar, R., Sathya, A.B., Vasantharaj, K., Sivasubramanian, V., 2014. Magnetic composite and environmental super adsorbent for dye sequestration - A review. Env. Nanotech., Monitoring & Management, 1-2, 36-49.

Smedley, P.L., Kinniburgh D.G., 2002. A review of the source, behaviour and distribution of arsenic in natural waters. Appl. Geochem. 17, 517–568.

Stumm W. and Bilinski H., 1972. Trace metals in natural waters, Proceeding of the 6th International Conference on Water Pollution Research, Pergamon Press, New York.

Suzuki M. 1990 *Adsorption Engineering*, 4th edn, Kodansha, Tokyo.

Thiebault, T. Guégan, R. Boussafir, M. 'Adsorption Mechanisms of Emerging Micro-pollutants with a clay Mineral: Case of Tramadol and Doxepine Pharmaceutical Products' J. Colloid Interface Sci., 453 1-8 (2015).

Tuna, A.Ö.A., Özdemir, E., Şimşek, E.B., Beker, U., 2013. Removal of As (V) from aqueous solution by activated carbon-based hybrid adsorbents: Impact of experimental conditions Chem. Eng. J. 223, 116–128.

Wang, X.S., Zhu, L., Lu H.J., 2011. Surface chemical properties and adsorption of Cu (II) on nanoscale magnetite in aqueous solutions. Desalination 276, 154–160.

Wiatrowski, H.A., Das, S., Kukkadapu, R., Ilton, E., Barkay, T., Yee, N., 2009. Reduction of Hg (II) to Hg (0) by magnetite. Environ. Sci. Technol. 43, 5307–5313.

Yang, G., Liu, Y., Song, S., 2015.Competitive adsorption of As(V) with co-existing ions on porous hematite in aqueous solutions. J. Environ. Chem. Eng. 3, 1497–1503

Yang, K., Peng, H., Wen, Y., Li, N., 2010. Re-examination of characteristic FTIR spectrum of secondary layer in bilayer oleic acid-coated Fe3O4 nanoparticles. Appl. Surf. Sci. 256, 3093–3097.

Yavuz, C.T., Mayo, J.T., Yu, W.W., Prakash, A., Falkner, J.C., Yean, S., Cong, L., Shipley, H.J., Kan, A., Tomson, M., Natelson, D., Colvin, V.L., 2006. Low-Field Magnetic Separation of Monodisperse Fe3O4 Nanocrystals. Science 314, 964-967.

Zakaria, A.K.M., Asgar M.A., Eriksson S.G., Ahmed FU, Yunus S.M., Azad A.K., Rundlof H., 2003. Preparation of Zn substituted Ni–Fe–Cr ferrites and study of the crystal structure by neutron diffraction. Mater. Lett. 57, 4243–4250.

Zhang, G., Qu, J., Liu, H., Liu, R., Wu, R., 2007. Preparation and evaluation of a novel Fe–Mn binary oxide adsorbent for effective arsenite removal. Water. Res. 41, 1921-1928.

Zhu, J., Baig, S.A., Sheng, T., Lou, Z., Wang, Z., Xu, X., 2015. Fe_3O_4 and MnO_2 assembled on honeycomb briquette cinders (HBC) for arsenic removal from aqueous solutions. J. Hazard. Mater. 286, 220–228.

Web references

http://maud.radiographema.eu/2016.05.05

http://water.epa.gov/drink/contaminants/basicinformation/copper.cfm#What are EPA's drinking water regulations for copper? 2015.09.08.

http://www.conserve-energy-future.com, 2015.09.08.

http://www.odor.net/carbon-adsorption/